A study on combining a multi-aperture interferometric imaging spectrometer with a multispectral camera

Daniele Picone, Mohamad Jouni, Mauro Dalla Mura

A STUDY ON COMBINING A MULTI-APERTURE INTERFEROMETRIC IMAGING SPECTROMETER WITH A MULTISPECTRAL CAMERA

Daniele Picone, Mohamad Jouni, Mauro Dalla Mura

Univ. Grenoble Alpes, CNRS,
Grenoble INP, GIPSA-lab,
38000 Grenoble, France

ABSTRACT

This work focuses on an image fusion protocol that combines conventional RGB cameras with multi-aperture devices utilizing Fabry-Perot interferometry, an unconventional way to acquire hyperspectral data with various advantages compared to dispersive spectrometers. The proposed system aims to enhance hyperspectral imaging quality by preserving high-resolution details from conventional cameras while incorporating the specific spectral range captured by the interferometric device, which mitigates the drawbacks associated to the difficulty of manufacturing Fabry-Perot etalons with low thickness. Envisioned for deployment on unmanned aerial vehicles (UAVs) and microsatellites, this compact setup holds promise for applications in environmental monitoring, agriculture, disaster management, and urban planning. The study presents theoretical foundations, addresses challenges, and offers preliminary results, demonstrating the effectiveness of the proposed approach through Bayesian inference.

***Index Terms*—** Hyperspectral data, Interferometry, Optimization, Image fusion.

1. INTRODUCTION

Advancements in remote sensing technologies have paved the way for more comprehensive and accurate data acquisition for remote sensing. In this work, we introduce a novel image fusion protocol to combine the capabilities of conventional cameras, such as RGB, with the more recently proposed designs for multi-aperture image spectrometers based on the interferometry of Fabry-Perot, aiming to enhance the overall imaging quality of the final product [1, 2, 3, 4, 5, 6].

Conventional cameras provide high-resolution color imagery over a limited amount of channels. Simultaneously, the multi-aperture device, based on Fabry-Perot interferometry principles [7], offers unique advantages in capturing specific spectral bands and increasing the sensitivity to targeted wavelengths [8, 9]. Their complementary information can be employed to implement a fusion step for processing the image; this composite image aims to not only preserve the high-resolution details from the conventional camera, but also inject the spectral information contained in the sub-images of the multi-aperture system. An example of the envisioned system is shown in Figure 1, which showcases a classic high resolution image (HRI) acquisition, in this case a multispectral (MS) image, which is paired up with a multi-aperture acquisition in the interferometric domain, with the final goal to reconstruct a fused product with the spatial resolution of the HRI and the finer spectral resolution made available through the interferometric domain representation.

The proposed approach offsets one of the most well-known drawbacks of Fabry-Perot interferometric systems, that is the difficulty to physically manufacture etalons with low thickness, which are associated to the low oscillation components of the reconstructed spectrum. That information can be partially recovered through the conventional camera acquisitions.

As both cameras are relatively compact and able to capture in snapshot mode, the envisioned setup is mostly aimed to be embedded on unmanned aerial vehicles (UAVs) and microsatellites. Potential applications range from environmental (especially gas) monitoring and agriculture to disaster management and urban planning. The proposed image fusion system holds promise for delivering richer, more informative datasets that can significantly improve decision-making processes in a variety of domains.

This work outlines the theoretical foundations, open challenges, and preliminary results of the proposed image fusion system. Specifically, we aim to demonstrate the effectiveness and versatility of our approach with some preliminary result employing Bayesian inference to obtain the desired product. We also aim to outline the potential problem statements that would be introduced by replicating this setup for real applications. This includes the problem of coregistering the snapshots, parametrizing the reconstruction algorithm, and choosing the scale ratio between the instruments.

Mauro Dalla Mura is also with Institut Universitaire de France (IUF), 75005 Paris, France. This work is partly supported by grant ANR FuMultiSPOC (ANR-20-ASTR-0006), and partly by Région Auvergne-Rhône-Alpes grant "Pack Ambition International 2021" (21-007356-01FONC, 21-007356-02INV).

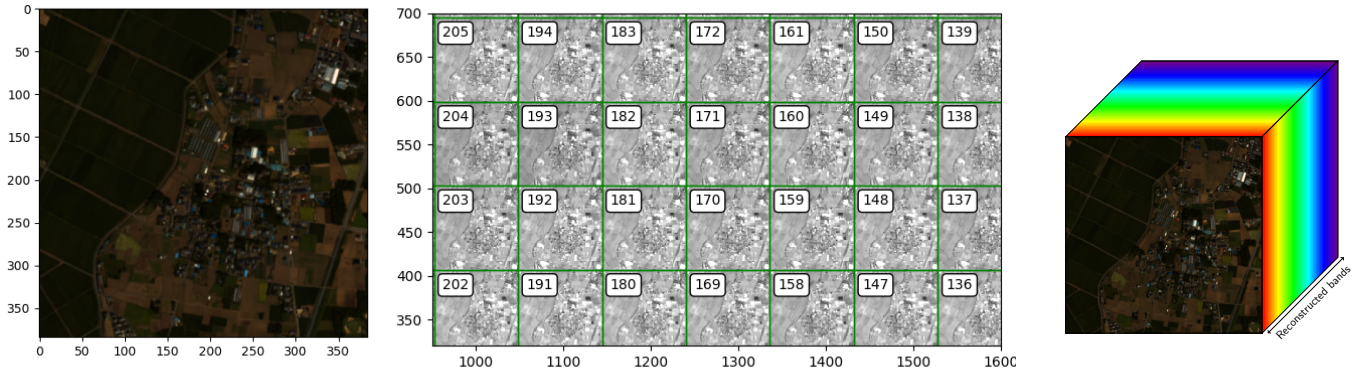

(a) Multispectral image (b) Image spectrometer acquisition (c) Reconstructed product

Fig. 1. Example of an acquisition of the coordinate fusion system and associated ideal product. The simulated acquisitions are obtained using the Chikusei dataset [10].

2. PROBLEM STATEMENT

For our purposes, we denote by $\mathbf{X} \in \mathbb{R}^{I \times J}$ the ideal reconstructed product, where I denotes the number of pixels of the conventional camera, while J denotes the amount of reconstructed channels. Additionally, the acquisition of the conventional camera is denoted by $\mathbf{M} \in \mathbb{R}^{I \times K}$, where $K < J$ being the respective number of channels. The acquisition of the multi-aperture image spectrometer, composed of L interferometers of different thicknesses, is denoted as $\mathbf{H} \in \mathbb{R}^{\frac{I}{\rho^2} \times L}$, where ρ defines the scale ratio in the spatial dimensions.

We then set up the reconstruction problem as follows:

$$\hat{\mathbf{X}} = \arg\min_{\mathbf{X}} \|\mathbf{X}\mathbf{R}^{\mathsf{T}} - \mathbf{M}\|_F^2 + \lambda_1 \|\mathbf{S}\mathbf{X}\mathbf{A}^{\mathsf{T}} - \mathbf{H}\|_F^2 + \lambda_2 \phi(\mathbf{X}) \quad (1)$$

where $\mathbf{R} \in \mathbb{R}^{K \times J}$ is the matrix of spectral degradation, $\mathbf{S} \in \mathbb{R}^{\frac{I}{\rho^2} \times I}$ is the matrix of spatial degradation (including blurring and downsampling), while $\mathbf{A} \in \mathbb{R}^{L \times J}$ is the matrix of transmittance response function of the image spectrometer. $\phi(\mathbf{X}) : \mathbb{R}^{I \times J} \to \mathbb{R}^{+}$ denotes the regularization function, introduced in order to counteract the ill-posedness/ill-conditioning of the problem. Additionally $\|\cdot\|_F$ represents the Frobenius norm.

One can easily recognize that, if $\mathbf{A}$ is an identity matrix, the cost function is equivalent to the joint optimization framework for hyperspectral sharpening [11].

In ideal conditions, as described in [6], the elements a_{lj} of $\mathbf{A}$ can be described by the Airy distribution [7, 12]; that is, up to a multiplicative factor:

$$a_{lj} = \left(1 + \frac{4\mathfrak{F}^2}{\pi^2} \sin^2\left(\pi \delta_l \sigma_j\right)\right)^{-1} \quad (2)$$

where $\mathfrak{F}$ is the finesse of the interferometer, and δ_l is the optical path difference (OPD) associated to the l-th interferometer. Here, σ_j denotes the j-th wavenumber which we wish to reconstruct, or in other words, the reciprocal of the j-th wavelength.

The OPD $\delta_l = 2nd_l \cos\theta$ is a function of the refraction index n and the thickness d_l of the cavity, as well as the angle of internal reflection θ.

3. EXPERIMENTS

In this section we aim to include experiments involving a series of different strategies for image fusion with interferometric data, employing a limited selection of regularizers.

In particular, we employ in this work a reference image, consisting of a cropped image from the Chikusei hyperspectral dataset, whose specifications are described in [10]. The dataset was equalized to the same dynamic range with the spectral information interpolated to be represented in a regularly sampled interval of wavenumbers $[1, 2.75]$ $\mu\mathrm{m}^{-1}$. The resulting reference image is then consisting of 200×200 pixels with 204 channels.

We then simulate the pair of observation: the HRI $\mathbf{M}$ and the interferometric acquisition $\mathbf{H}$. The HRI is simulated using the spectral responses of the Worldview-2 (WV2) satellite as the spectral degradation matrix $\mathbf{R}$; since WV2 platforms are equipped with both a panchromatic and a MS sensor, the HRI can be either monochromatic or consist of 8 bands.

The interferometric acquisition is simulated with two steps: first the reference is downsampled by a scale factor $\rho = 4$ using a Gaussian blurring kernel with Nyquist gain of 0.28, and then the spectral domain is transformed to an

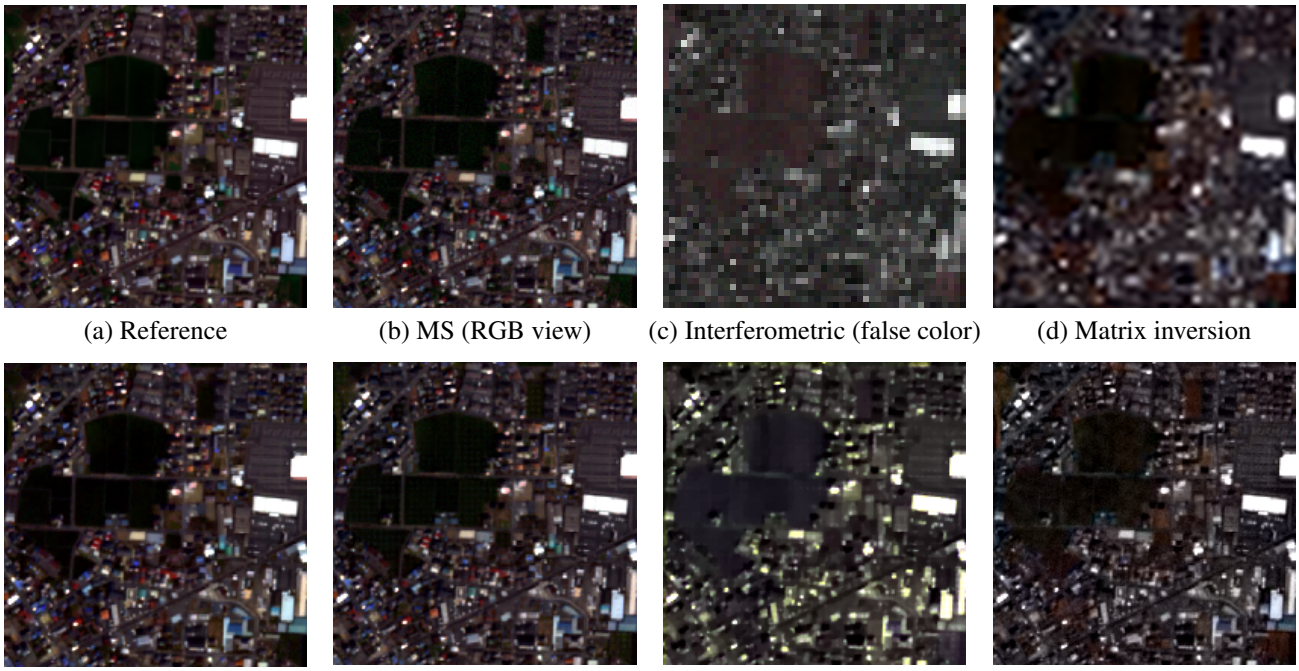

(a) Reference (b) MS (RGB view) (c) Interferometric (false color) (d) Matrix inversion

(e) Joint w/ MS (f) Sequential w/ MS (g) Joint w/ PAN (h) Sequential w/ PAN

Fig. 2. Results for the fusion of interferometric acquisition for the Chikusei dataset with MS and PAN used as HRI. The reference and reconstructed datacubes are represented using the wavenumber equivalents of the channels $[60, 40, 20]$ as their RGB.

interferogram. This choice is typical for other works on data fusion as this blurring kernel is often used as representation of the point spread function (PSF) of the acquisition system, which in our case correspond to that of the focal plane array of the multi-aperture inteferometer.

For this last step, the trasmittance response $\mathbf{A}$ uses a finesse $\mathfrak{F} = 1.75$ and we use a set of optical path differences (OPDs) which covers a range of $[0, 80]\mu\mathrm{m}$ and is regularly spaced with a step size of $0.25\mu\mathrm{m}$. This configuration loosely replicates the one of the prototype proposed in [1] and also used in the experimental section of [9].

Both $\mathbf{R}$ and $\mathbf{A}$ were normalized to sum-to-1 over columns and we added white Gaussian noise to the obtained observation such that the SNR is equal to 20 dB. This is the usual level of noise that we can find on optical sensors.

We then compare several strategies to fuse data. Whenever we use the Bayesian framework of eq. (1), the problem is resolved through the Loris-Verhoeven solver [13], using $\lambda_1 = 1$ and $\lambda_2 = 0.0025$, while letting the algorithm run for 1000 iterations. We employ a regularizer $\phi(\cdot)$ that applies total variation, calculating gradients over the spatial dimensions, and then applies over the spectral ones. Then the ℓ_2 norm is applied over the gradients and ℓ_1 over all the other axis of the datacube.

The algorithm is applied under two scenarios, in the *joint* scenario, the algorithm is run as it is, while in the *sequential* scenario the algorithm is solved in two steps.

- We perform a standard matrix inversion reconstruction to find an estimation $\widehat{\mathbf{B}}$ of the hyperspectral image at reduced resolution:

$$\widehat{\mathbf{B}} = \arg\min_{\mathbf{B}} \|\mathbf{B}\|_F^2 + \lambda_2 \phi(\mathbf{B}) \tag{3}$$

- We perform a standard fusion between $\widehat{\mathbf{B}}$ and the HRI $\mathbf{M}$, solving eq. (1), with the transmittance response $\mathbf{A}$ set as identity.

We hence can define 4 different scenarios, combining the joint and sequential settings and using either the MS or the panchromatic as the HRI. For completion, we also provide the results of reconstruction when no HRI is available, where we substituted the second step of the sequential procedure with a spatial interpolation using a 23-tap kernel [14]. This is labeled as "matrix inversion" in the following.

The results are shown in Table 1 and a visualization is shown in Figure 2.

A quick analysis shows that the availability of a MS image is much more beneficial to the reconstruction over a simple panchromatic (PAN), although some color distortions still remains, which are quite evident especially by analyzing the colors on the road. In both cases, the spatial resolution is

Method	PSNR	SSIM	SAM
Ideal	∞	1	0
Joint w/ MS	24.22	0.8658	13.61
Sequential w/ MS	**26.07**	**0.8691**	**11.08**
Sequential w/ PAN	20.96	0.6892	18.78
Matrix inversion	18.36	0.4098	17.51

Table 1. Performance metrics for different methods on Chikusei dataset. The definition of the quality indices employed in this table are provided in [15, 16]. Best results in bold.

much improved with respect to the simple matrix inversion, acting here as baseline, although the fusion with the PAN does not necessarily imply that the spectral component is not distorted.

Somewhat surprisingly, the proposed algorithm was not able to perform better than when the data is processed separately, even if both steps of the algorithm are specializations of the same basic formulation. We speculate that this effect is due to the increased complexity of the problem, so that the convergence of the separate problem is faster than the joint one.

4. CONCLUSIONS

The problem of inversion of interferometric acquisitions for the recovery of spectra is still an open issue for the community of Fourier transform imaging spectrometers. The main challenges arise in the complexity of the reconstruction algorithm and in the challenge manufacturing complexity of imaging devices that are capable to provide a full interpolation of the interferogram. This challenges have not allowed the community to recover the full hyperspectral datacubes to be used in various tasks for remote sensing applications.

In this paper, we present a viable alternative to complement this data, demonstrating how the availability of multispectral data drastically improves our capability to resolve spatial and spectral characteristics of the scene. This proof of concept may for example justify the necessity of installing a standard RGB camera to complement the image spectrometer, for example for unmanned aerial vehicless (UAVs) if the weight is within its payload.

While the joint approach was not able to provide convincing results, the availability of the Bayesian framework still allows to dynamically separate the problem into its component parts.

However this result still depends on the capability of the user to properly represent the characteristics of the acquisition system, such as that of the spatial blurring kernel, of the spectral responses of the high resolution camera, and of the transmittance response of the image spectrometer.

Additionally, potential issues still remains related to the spatial coregistration among the two cameras, and an accurate selection of the scale ratio between the ground sample distance of the two devices.

5. REFERENCES

[1] Marco Pisani and Massimo E. Zucco, "Compact imaging spectrometer combining Fourier transform spectroscopy with a Fabry-Perot interferometer," *Optics Express*, vol. 17, no. 10, pp. 8319–8331, May 2009.

[2] Massimo Zucco, Marco Pisani, Valentina Caricato, and Andrea Egidi, "A hyperspectral imager based on a Fabry-Perot interferometer with dielectric mirrors," *Optics Express*, vol. 22, no. 2, pp. 1824–1834, Jan. 2014.

[3] Yaniv Oiknine, Isaac August, and Adrian Stern, "Multi-aperture snapshot compressive hyperspectral camera," *Optics Letters*, vol. 43, no. 20, pp. 5042–5045, Oct. 2018.

[4] Silvère Gousset, Laurence Croizé, Etienne Le Coarer, Yann Ferrec, Juana Rodrigo Rodrigo, Laure Brooker, et al., "NanoCarb hyperspectral sensor: On performance optimization and analysis for greenhouse gas monitoring from a constellation of small satellites," *CEAS Space Journal*, vol. 11, no. 4, pp. 507–524, 2019.

[5] Nicolas Guerineau, Etienne Le Coarer, Yann Ferrec, and Florence De La Barriere, "Fourier transform multi-channel spectral imager," Jan. 2018, FR patent 1,656,162.

[6] Daniele Picone, Silvère Gousset, Mauro Dalla Mura, Yann Ferrec, and Etienne le Coarer, "Interferometer response characterization algorithm for multi-aperture Fabry-Perot imaging spectrometers," *Optics Express*, vol. 31, no. 14, pp. 23066–23085, June 2023.

[7] Gonzalo Hernández, *Fabry-Perot interferometers*, Number 3. Cambridge University Press, 1988.

[8] Mohamad Jouni, Daniele Picone, and Mauro Dalla Mura, "Model-based spectral reconstruction of interferometric acquisitions," in *IEEE International Conference on Acoustics, Speech and Signal Processing (ICASSP)*. June 2023, pp. 1–5, IEEE.

[9] Daniele Picone, Mohamad Jouni, and Mauro Dalla Mura, "Spectro-spatial hyperspectral image reconstruction from interferometric acquisitions," in *IEEE International Conference on Acoustics, Speech and Signal Processing (ICASSP)*. Apr. 2024, IEEE.

[10] Naoto Yokoya, Claas Grohnfeldt, and Jocelyn Chanussot, "Hyperspectral and multispectral data fusion: A comparative review of the recent literature," *IEEE Geoscience and Remote Sensing Magazine*, vol. 5, no. 2, pp. 29–56, June 2017.

[11] Gemine Vivone, "Multispectral and hyperspectral image fusion in remote sensing: A survey," *Information Fusion*, vol. 89, pp. 405–417, Jan. 2023.

[12] Parameswaran Hariharan, *Basics of interferometry*, Elsevier, 2010.

[13] Ignace Loris and Caroline Verhoeven, "On a generalization of the iterative soft-thresholding algorithm for the case of non-separable penalty," *Inverse Problems*, vol. 27, no. 12, pp. 125007, Nov. 2011.

[14] Bruno Aiazzi, Stefano Baronti, Massimo Selva, and Luciano Alparone, "Bi-cubic interpolation for shift-free pan-sharpening," *ISPRS Journal of Photogrammetry and Remote Sensing*, vol. 86, no. 6, pp. 65–76, Dec. 2013.

[15] Z. Wang, A. C. Bovik, H. R. Sheikh, and E. P. Simoncelli, "Image quality assessment: from error visibility to structural similarity," *IEEE Transactions on Image Processing*, vol. 13, no. 4, pp. 600–612, Apr. 2004.

[16] Roberta H. Yuhas, Alexander F. H. Goetz, and Joe W. Boardman, "Discrimination among semi-arid landscape endmembers using the spectral angle mapper (SAM) algorithm," in *Proc. Summaries 3rd Annu. JPL Airborne Geosci. Workshop*, 1992, vol. 1, pp. 147–149.